**Structural Engineering and Mechanics**, *Vol. 70, No. 1 (2019) 33-41*
DOI: https://doi.org/10.12989/sem.2019.70.1.033


# Influence of geometry and safety factor on fatigue damage predictions of a cantilever beam

Matija Pečnik[a], Marko Nagode[b] and Domen Šeruga*

*University of Ljubljana, Faculty of Mechanical Engineering, Aškerčeva 6, SI-1000 Ljubljana, Slovenia*

*(Received January 5, 2018, Revised August 9, 2018, Accepted February 8, 2019)*

**Abstract.** The influence of two parameters on fatigue damage predictions of a variably loaded cantilever beam has been examined. The first parameter is the geometry of the cantilever beam and the weld connecting it to a rear panel. Variables of the geometry examined here include the cantilever length, the weld width on the critical cross-section and the angle of the critical cross-section. The second parameter is the safety factor, as set out by the Eurocode 3 standard. An analytical approach has been used to calculate the stresses at the critical cross-section and standard rainflow counting has been used for the extraction of the load cycles from the load history. The results here suggest that a change in the width and angle of the critical cross-section has a non-linear impact on the fatigue damage. The results also show that the angle of the critical cross-section has the biggest influence on the fatigue damage and can cause the weld to withstand fatigue better. The second parameter, the safety factor, is shown to have a significant effect on the fatigue damage calculation, whereby a slight increase in the endurance safety factor can cause the calculated fatigue damage to increase considerably.

**Keywords:** fatigue damage; welded joint; rainflow; cantilever beam; fatigue

## 1. Introduction

Mechanical structures on both a large and small scale often include cantilever beams (Altunisik *et al.* 2016, Ingole and Chatterjee 2015). They can be used in large structures such as arch bridges (Granata *et al.* 2013), highway bridges (Altunisik *et al.* 2010), guardrail terminal systems, or for modelling wind turbine blades (Gonzalez-Cruz 2016). At the opposite end of the scale they are used in medicine for total hip arthroplasty (Griza *et al.* 2013, Fokter *et al.* 2017) or even on a micro scale as cantilever probe tips in atomic force microscopy (Korayem 2017). During operation cantilever beams are subjected to variable loading which can lead to fatigue failure (Saranik *et al.* 2013, Paulus and Dasgupta 2012, Schijve 2009), especially those beams used in automotive or agricultural industries where they usually operate in extremely dynamic conditions (Savković *et al.* 2011). Fatigue analyses are therefore mandatory in the development stage of mechanical structures to reduce the occurrence of fatigue failure (Šeruga *et al.* 2011, Anwar *et al.* 2017, Šeruga *et al.* 2014, Akrache and Lu 2011), which can originate from any form of crack (Zeng *et al.* 2017, Shi and Nakano 2001, Liu *et al.* 2016).

For welded cantilever beams, standards such as Eurocode 3 (Eurocode 2005) describe the procedure for the fatigue analyses, durability curves and safety factors involved in these analyses. The use of this safety concept is considered during the design of structures (Sedlacek and Kraus 2007).

In this study a cantilever beam used for the transport of a large mechanical device has been examined (Fig. 1(a)). The cantilever beam is made of two steel C-profiles (Fig. 2), welded facing each other with a butt weld.

Both profiles are then welded to a rear panel with a fillet weld. The load is applied on the free end with a force vector as shown in Fig. 1(a).

The variable load on the free end of the cantilever beam was measured and is now given as a factor f by which the nominal value of the force vector is multiplied during the measurement. This measurement (see Fig. 1(b)) has then been used as a block of load history for which the accumulated fatigue damage was calculated.

## 2. Methods

$$\sigma_{\perp}(x,y,z)=\frac{N(x)}{A}+\frac{I_y M_z(x)-I_{yz}M_y(x)}{I_y I_z-I_{yz}^2}y+\frac{I_z M_y(x)-I_{yz}M_z(x)}{I_y I_z-I_{yz}^2}z \tag{1}$$

The procedure is divided into two parts: a structural analysis and a fatigue analysis. The purpose of the structural analysis is to calculate the stress in the critical cross-section which occurs due to the nominal force. Assuming the stress is less than the yield strength of the material, the fluctuation of the stress at any given point in the beam resembles the

*Corresponding author, Assistant Professor
E-mail: domen.seruga@fs.uni-lj.si
[a]M.Eng Student
[b]Ph.D. Professor


http://www.techno-press.com/journals/sem&subpage=7

ISSN: 1225-4568 (Print), 1598-6217 (Online)

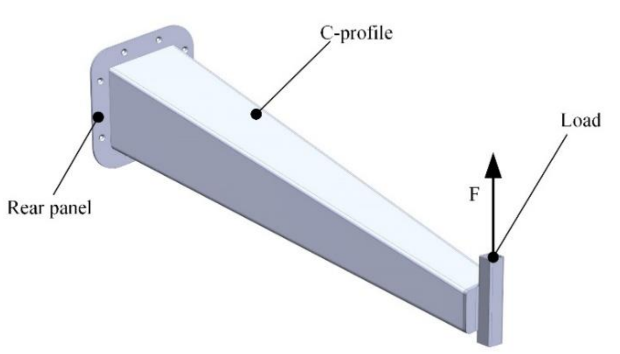


(a) Welded cantilever beam

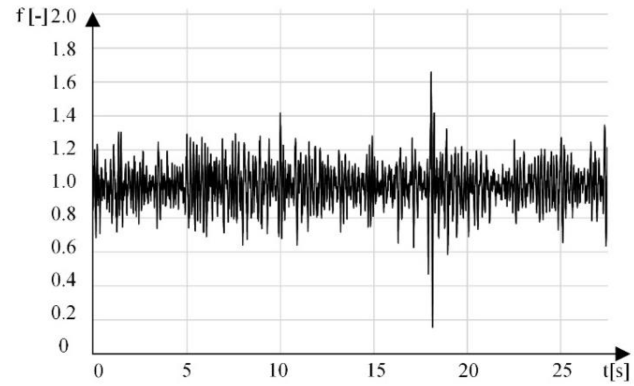


(b) Random load measurement

Fig. 1 Cantilever beam welded onto plate and loaded on the free end

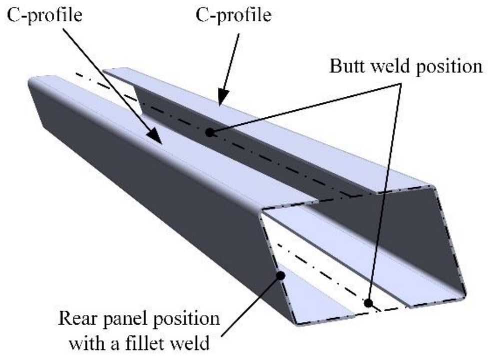


Fig. 2 Two steel C-profiles prepared for cantilever beam

fluctuation of the load signal. An analytical approach has been chosen for the structural analysis to calculate the nominal stress although a numerical analysis such as finite element analysis could be applied instead (Wang *et al.* 1995, Zaletelj *et al.* 2011, Iwicki *et al.* 2015, Sondej *et al.* 2016, Akrache and Lu 2011).

The purpose of fatigue analysis is to calculate the durability of material when it is subjected to repeated loading. The calculation uses normal stress, shear stress transverse to the axis of the weld and shear stress longitudinal to the axis of the weld. The system examined here is a cantilever beam of variable cross-section carrying a force F on the free end and being fixed to the rear panel at the other end (Fig. 1(a)).

### *2.1 Structural analysis*

The procedure for the structural analysis is summarised in Fig. 3. It starts with a simplification of the cantilever beam. A Cartesian coordinate system must be defined and positioned at the centre of gravity of the critical cross section. The highest stress in the cantilever beam is located in the cross-section furthest away from the position of the load (force vector) applied on the beam (Fig. 4(a)). For this cantilever beam, this cross-section is located at the same position as the fillet weld between the beam and the rear plate.

Following the simplification of the structure by transforming a whole cantilever beam to a welded cross-section and force vector form, analytical local stress calculations were carried out for 8 locations at the end of each side of the weld and labelled P1 to P8 (see Fig. 5).

Because the beam is under combined load, connection between it and local normal stress was established taking into account cross section's characteristics using Navier's equation (Eq. (1)).

Only the critical cross-section (Fig. 5) has been considered for the structural analysis. The cross-sectional area is defined by an angle $\alpha$ and width a (see Fig. 5).

After defining the combined centre, moments of inertia have been calculated for the cross-section. Components of the force vector have been reduced into respective moments around the centre of a Cartesian coordinate system (see Fig. 4(b)). By inserting the values of locations, moments and moments of inertia in Navier's equation (Eq. (1)), the normal stress is calculated for each of the eight locations.

The shear stress for longitudinal and transversal direction for each of the eight locations is calculated using Eq. (2) and Eq. (3), respectively, where $A_\mathrm{w}$ represents the area of the weld.

The shear stress due to torsion is calculated according to the equation for closed thin-wall sections (Eq. (4)). It is assumed that the section is closed, where $A_H$ is the area enclosed within the median line of the weld thickness, represented by the dashed line in Fig. 5.

$$\tau_{\parallel,i} = \frac{F_{\parallel,i}}{A_\mathrm{w}}, i = 1,...,8 \tag{2}$$

$$\tau_{\perp,i} = \frac{F_{\perp,i}}{A_\mathrm{w}}, i = 1,...,8 \tag{3}$$

$$\tau_{\parallel} = \frac{M_x}{2A_\mathrm{H}a} \tag{4}$$

All that is needed then is to recalculate the stress for each weld separately using the Eurocode 3 comparison-equation for relevant stresses, which also makes it ready for application.

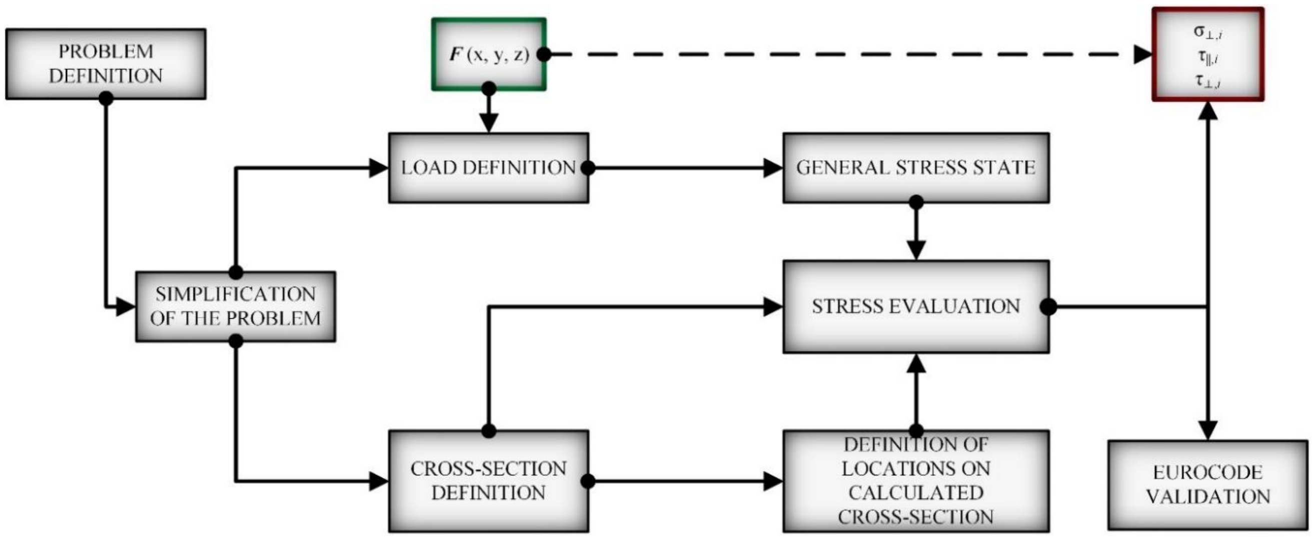


Fig. 3 Procedure of the structural analysis

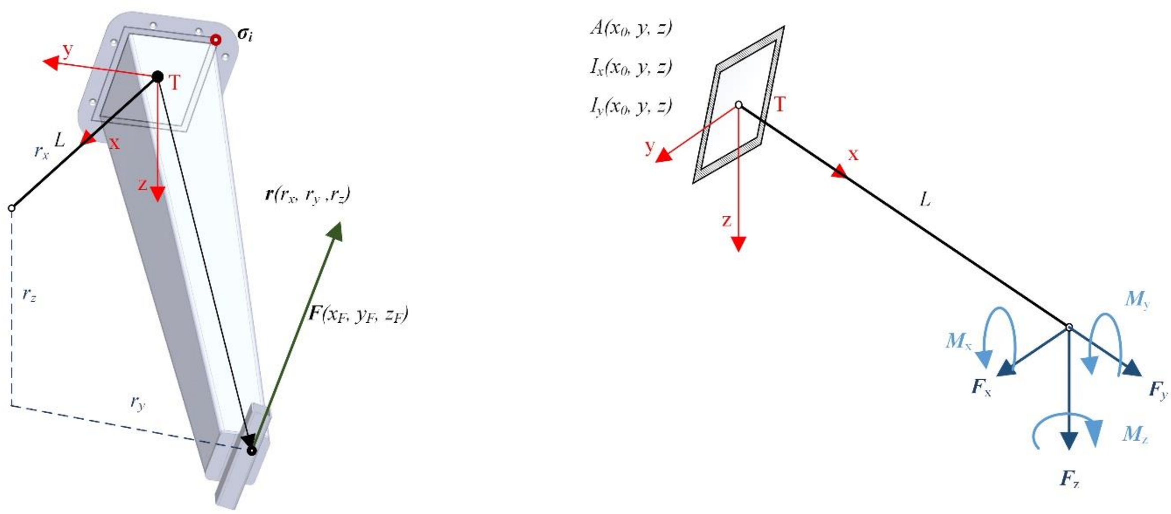


(a) Coordinate system and force vector (b) Reduced load

Fig. 4 Position of the force vector-load and the reduction of the load for easier calculation

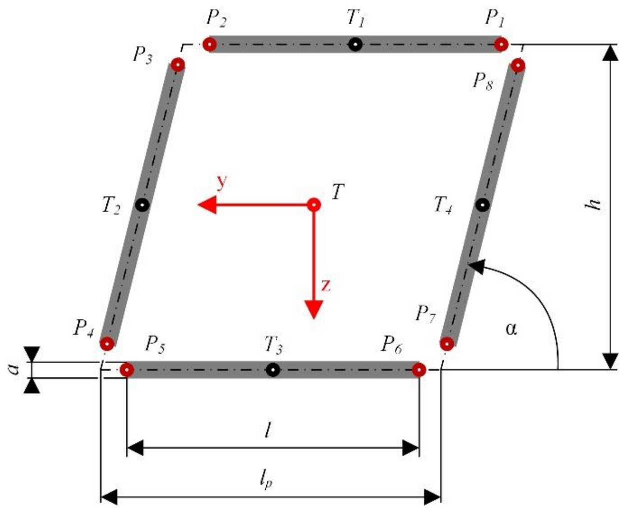


Fig. 5 Local stress locations on weld ends

### 2.2 Fatigue analysis

By defining specific relevant normal stress $\sigma_{wf}$ and relevant shear stress $\tau_{wf}$ for the chosen locations as a function of the applied load, we proceed with the assumption that varying the amplitude of this load affects the local stress-state linearly. This means that the local stress range varies proportionally to the block of loading history (Fig. 1).

$$\sigma_{\mathrm{wf}} = \sqrt{\sigma_{\perp} + \tau_{\perp}} \tag{5}$$

The relevant normal stress is calculated by considering the normal stress and the shear stress transverse to the axis of the weld (Eq. (5)) whilst the relevant shear stress is equal to the longitudinal shear stress.

The block of load history has been analysed using the rainflow method (Marsh *et al.* 2016), where an algorithm counts closed cycles that accumulate damage. The entire block of loading history is analysed and all closed cycles are counted. The counted ranked cycles are collected and used to define a stress range histogram. Each cycle also contributes to fatigue crack propagation (Totten 2008) and was inserted into Eq. (6) for calculation of the accumulated fatigue damage.

However, for the calculation of fatigue damage a constructional detail category has to be defined. The constructional detail category is dependent on the element's geometry and loading according to Eurocode 3. This specific constructional detail can be represented by a bi-linear Wöhler curve (which relates the relevant stress range and total number of cycles to failure) and its fatigue strength. For failure to occur, fatigue damage would be 100% or $D$=1 (Eq. (6)).

The procedure is shown in Fig. 6. By choosing the category of constructional detail according to Eurocode 3, the appropriate Wöhler curves for normal and shear stresses are chosen, respectively, and the fatigue damage is calculated (Fig. 7). For the damage calculation we have used the Palmgren-Miner linear damage accumulation rule (Nussbaumer *et al.* 2011, see Eq. (6))

$$D=\sum_{i=1}^{n}\frac{n_i(\Delta\sigma_{\mathrm{wf},i})}{N_i(\Delta\sigma_{\mathrm{wf},i})}+\sum_{i=1}^{n}\frac{n_i(\Delta\tau_{\mathrm{wf},i})}{N_i(\Delta\tau_{\mathrm{wf},i})} \tag{6}$$

The number of cycles to failure is calculated according to the slope of the Wöhler curve (Eqs. (7)-(9)).

$$N_i(\Delta\sigma_{\mathrm{wf},i})=\left(\frac{\frac{\Delta\sigma_{\mathrm{D}}}{\gamma_{\mathrm{Mf}}}}{\Delta\sigma_{\mathrm{wf},i}}\right)^m 5\times10^6;\ m=3,\ \frac{\Delta\sigma_{\mathrm{D}}}{\gamma_{\mathrm{Mf}}}\le\Delta\sigma_{\mathrm{wf},i} \tag{7}$$

$$N_i(\Delta\sigma_{\mathrm{wf},i})=\left(\frac{\frac{\Delta\sigma_{\mathrm{D}}}{\gamma_{\mathrm{Mf}}}}{\Delta\sigma_{\mathrm{wf},i}}\right)^m 5\times10^6;\ m=5,\ \frac{\Delta\sigma_{\mathrm{L}}}{\gamma_{\mathrm{Mf}}}\le\Delta\sigma_{\mathrm{wf},i}<\frac{\Delta\sigma_{\mathrm{D}}}{\gamma_{\mathrm{Mf}}} \tag{8}$$

$$N_i(\Delta\tau_{\mathrm{wf},i})=\left(\frac{\frac{\Delta\tau_{\mathrm{D}}}{\gamma_{\mathrm{Mf}}}}{\Delta\tau_{\mathrm{wf},i}}\right)^m 5\times10^6;\ m=5,\ \frac{\Delta\tau_{\mathrm{L}}}{\gamma_{\mathrm{Mf}}}\le\Delta\tau_{\mathrm{wf},i} \tag{9}$$

All relevant stress ranges below cut off stresses of $\Delta\sigma_L$ and $\Delta\tau_L$ are considered to not cause any damage (Eqs. (10) and (11))

$$N_i=\infty,\qquad \frac{\Delta\sigma_{\mathrm{L}}}{\gamma_{\mathrm{Mf}}}>\Delta\sigma_{\mathrm{wf},i} \tag{10}$$

$$N_i=\infty,\qquad \frac{\Delta\tau_{\mathrm{L}}}{\gamma_{\mathrm{Mf}}}>\Delta\tau_{\mathrm{wf},i} \tag{11}$$

The Eurocode 3 standard uses a partial endurance safety factor $\gamma_{Mf}$, which decreases all values of the Wöhler curve in Fig. 6. These values are carefully defined in Eurocode 3 and should be considered in the process of the fatigue life calculation (Table 1).

Table 1 Recommended values for $\gamma_{Mf}$

| Assessment method | Consequence of failure | |
|---|---|---|
| | Low consequence | High consequence |
| Damage tolerant | 1.00 | 1.15 |
| Safe life | 1.15 | 1.35 |

Table 2 Nominal load and position of load vector

| Position of the force-load | mm | Force-vector components | N |
|---|---|---|---|
| $r_x$ | 928 | $F_x$ | -1349 |
| $r_y$ | -1121 | $F_y$ | 0 |
| $r_z$ | 448 | $F_z$ | -8898 |

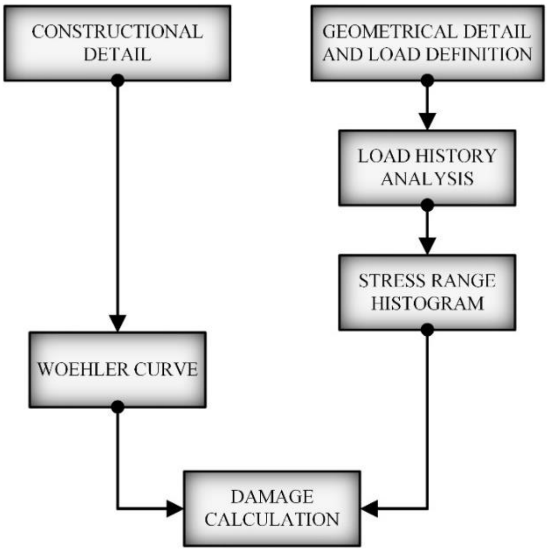


Fig. 6 Fatigue damage calculation procedure

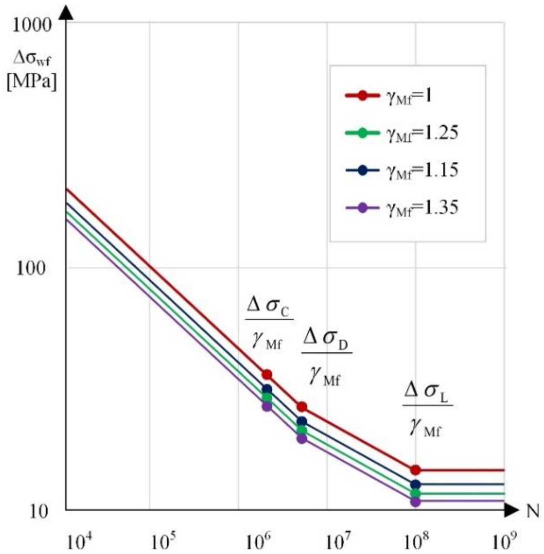


Fig. 7 Wöhler curve for normal stress with different safety factors

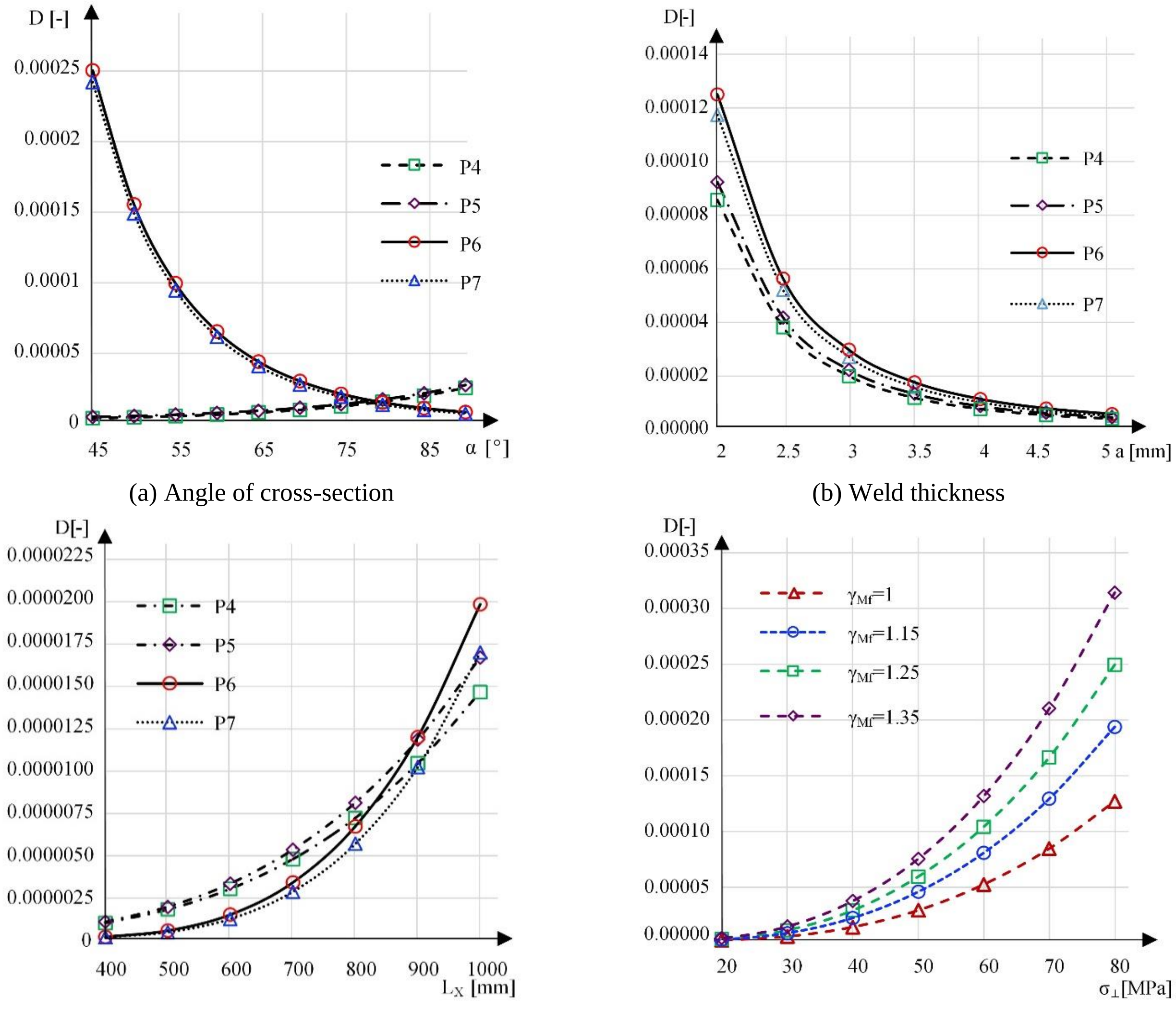


(a) Angle of cross-section

(b) Weld thickness

(c) Length – x coordinate

(d) Endurance safety factor

Fig. 9 The influence of angle of cross-section, weld thickness, length and safety factor on the fatigue damage for the given block of loading history

Table 3 Initial values defining the geometry of the cross-section

| Parameter | Value |
|---|---|
| *a* | 3.5 mm |
| *l* | 211 |
| *α* | 76.5° |
| *h* | 218 mm |

## 3. Results and discussion

In our example, the nominal value of the applied load F is 9000 N and is positioned according to the Cartesian coordinate system (see Fig. 4(a)) and Table 2.

Initially, the shape of the cross-section where the beam is welded onto the fixed plate is defined as a parallelogram (Table 3). All sides are the same length, which defines the position of the welds in a rhombus shape, where each of the welds is slightly shorter than the length of the side of the rhombus (see Fig. 5).

Table 4 Stresses in critical locations

| Location number | Normal stress $\sigma_{\perp}$ [MPa] | Transversal shear stress $\tau_{\perp}$ [MPa] | Longitudinal shear stress $\tau_{\parallel}$ [MPa] |
|---|---|---|---|
| P1 | -35.75 | -0.26 | -1.88 |
| P2 | -39.59 | -0.26 | -1.88 |
| P3 | -38.46 | -0.64 | -1.93 |
| P4 | -33.58 | -0.64 | -1.93 |
| P5 | -34.84 | 0.64 | 1.88 |
| P6 | 38.68 | 0.64 | 1.88 |
| P7 | 37.54 | 0.27 | 1.84 |
| P8 | -34.49 | 0.27 | 1.84 |

The angle $\alpha$ of the cross-section (Table 3) can range from 45 to 90°. For 90° the welds lie along the edges of a square. The highest normal stresses from structural analysis on the critical cross-section occur at locations P4, P5, P6 and P7 (Fig. 5 and Table 4). Therefore, the highest fatigue

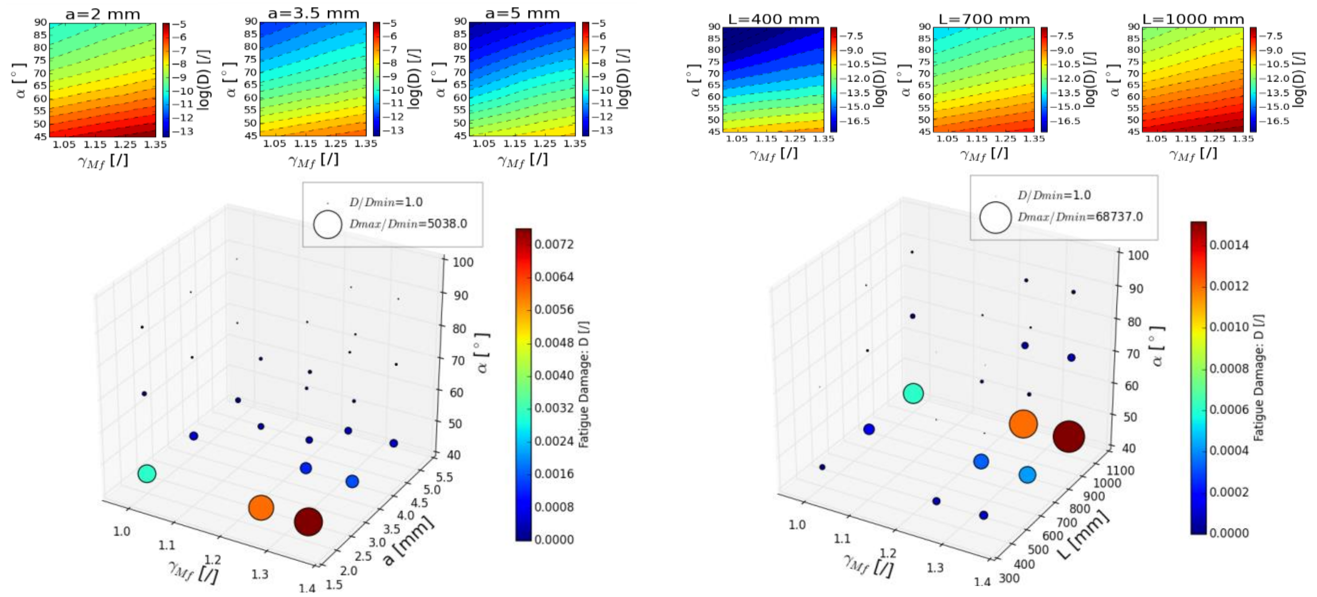


(a) L=1000 mm, angle ($\alpha$), weld width (a) and endurance safety factor ($\gamma_{Mf}$)

(b) a=3.5 mm, angle ($\alpha$), length (L) and endurance safety factor ($\gamma_{Mf}$)

Fig. 10 Calculated fatigue damage for the combination of variables at location P6. Each combination of the variables is represented by a circle in 3D diagrams. The colour of the circle indicates the value of the computed fatigue damage. The size of the circle represents the calculated fatigue damage relative to the minimal calculated fatigue damage shown in the diagram. 2D diagrams are given for the chosen (a) weld widths and (b) lengths. Logarithmic scale of damage is used in 2D diagrams for a clearer presentation of the results

Table 5 Parameter and variable ranges

| Variable | Range | | | | | | | | | |
|---|---|---|---|---|---|---|---|---|---|---|
| $L_x$ [mm] | 400 | 500 | 600 | 700 | 800 | 900 | 1000 | / | / | / |
| $a$ [mm] | 2 | 2.5 | 3 | 3.5 | 4 | 4.5 | 5 | / | / | / |
| $\alpha$ [°] | 45 | 50 | 55 | 60 | 65 | 70 | 75 | 80 | 85 | 90 |
| $\gamma_{Mf}$ | 1.0 | 1.15 | 1.25 | 1.35 | / | / | / | | / | / |

damage is calculated for these locations regardless of the variation of the parameters.

For each location number the calculated stress (Table 4) is multiplied by the measured load history, which equals the stress history.

Because the measured block of load history is always above zero (see Fig. 1(b)), every stress at the chosen locations has the same sign as stress in the structural analysis. The damage calculated with these principles represents the damage accumulated by one block of loading history (Fig. 1) in the location with the highest positive normal stress (Table 4), whereby negative normal stress is not so critical for crack propagation (Eurocode 3).

For the cantilever beam the constructional detail category is taken to be $\Delta\sigma_C$ with a normal stress range of 36 MPa, which defines the entire Wöhler curve (Fig. 7) and $\Delta\tau_C$ with a shear stress range of 80 MPa (Eurocode 3). This detail is based on the type of load, the position of the work piece and the joint between the cantilever and the back plate which in this case is considered to be a fillet welded tee joint.

It can also be observed that the studied cantilever is not ideally welded perpendicular to the back plate. It should also be mentioned that the proposed construction detail that represents the endurance curves has the lowest normal and shear stress range possibility covered by the Eurocode 3.

Initial values of the variables of the geometry (cantilever length, weld width on the critical cross-section, angle of critical cross-section) and the safety factor have been chosen as given in Table 3. To illustrate, the relevant normal stress range $\Delta\sigma_{wf,a}$=20.74 MPa is obtained at location P6 using the rainflow method (see Fig. 8(a)), which was applied for the block of load history multiplied by the stresses calculated using Eqs. (1)-(5). All relevant normal stress ranges have been collected to form a relevant normal stress range histogram (see Fig. 8(b)). The value in this example can be found in the relevant normal stress range histogram with ranked stresses slightly above 20 MPa (Fig. 8(b)). This relevant normal stress range repeats 7 times in the stress history, which defines $n_a$=7. After the application of the safety factor $\gamma_{Mf}$=1.25, an adjusted constant amplitude fatigue limit ($\Delta\sigma_D$) of 21.2 MPa is obtained. Therefore, the cycles to failure have been calculated using the following equations (Eqs. (12)-(14)).

$$N_a = 5\times10^6\left(\frac{\frac{\Delta\sigma_D}{\gamma_{Mf}}}{\Delta\sigma_{wf,a}}\right)^5 \tag{12}$$

$$N_a = 5\times10^6\left(\frac{21.22}{20.74}\right)^5 \tag{13}$$

$$N_a = 5606001 \tag{14}$$

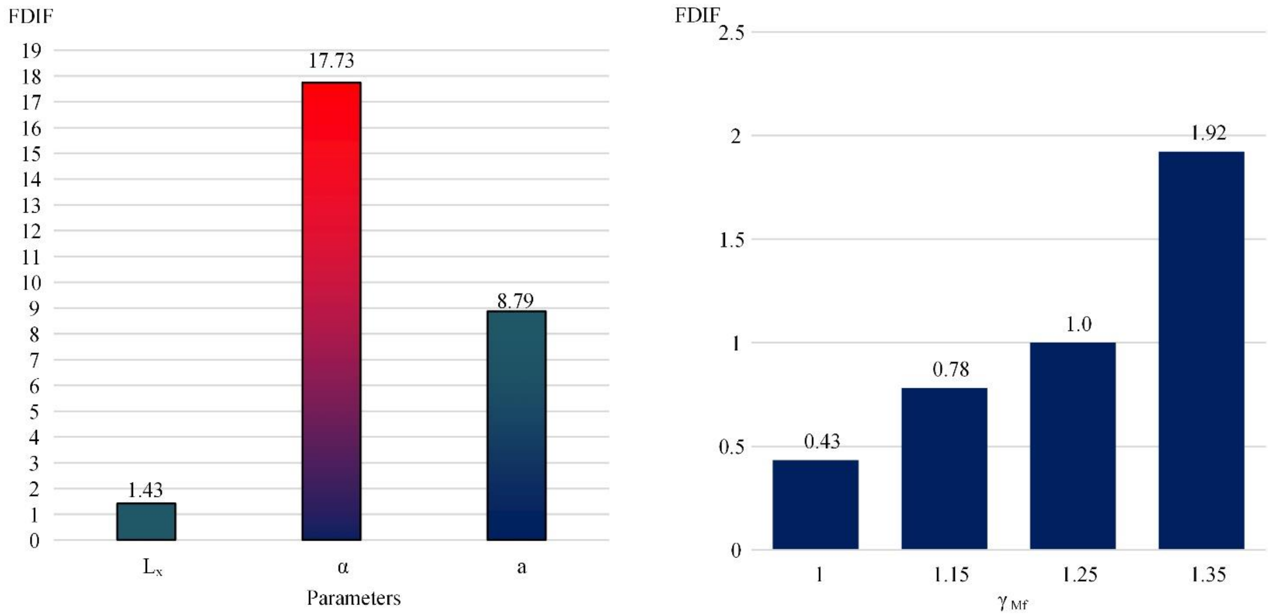


(a) Fatigue damage impact of geometric variables: length ($L_x$), angle ($\alpha$) and weld width (a)

(b) Endurance safety factor ($\gamma_{Mf}$)

Fig. 11 Impact of geometry and safety factor on fatigue damage

Using the Palmgren-Miner rule (Eq. (6)) and calculated cycles to failure (Eq. (14)), the damage caused by this particular relevant normal stress range can be calculated as (Eq. (15))

$$D_a = \frac{n_a}{N_a} = \frac{7}{5606001} = 1.25 \times 10^{-6} \tag{15}$$

For the calculation of fatigue damage due to relevant shear stresses, Eq. (11) is used. As all the values of relevant shear stresses lie beneath the cut-off stress, the damage equals zero.

The calculated damage with the initial values of the parameters for the entire block of load history results in $D_0=1.65\times10^{-5}$. This value is considered as the initial fatigue damage value for the purpose of comparison. The damage calculated in Eq. (15) uses a safety factor $\gamma_{Mf}$ of 1.25. The safety factor was then varied from 1.0 to 1.35 (Table 3) and the resulting damage compared (see Fig. 9(d)).

The study has compared the following parameters: geometry of the cantilever and critical cross-section and partial endurance safety factor "$\gamma_{Mf}$". For the geometry, the following variables were looked at: weld width "a", cantilever beam length "l", and angle of cross-section "α". The influence of parameters or variables was studied in the range of values shown in Table 5.

The weld width "a" was varied from the maximum allowable value for the selected thickness of the sheet metal (5 mm) to 40 % of this value. The length "l" of the cantilever beam was varied only in the longitudinal direction while the other two dimensions remained the same. This way, only $M_y$ changes, while $M_x$ and $M_z$ remain the same.

In Fig. 9(a), it can be seen that by increasing the angle $\alpha$, the calculated damage of locations P6 and P7 decreases, whilst that at locations P4 and P5 it increases. This suggests that there exists an optimal angle for which the fatigue damage is minimal. Of course, this assumption is only true for the given block of load history, the shape of the cross-section and the load. In Fig. 9(b), a decrease in the fatigue damage is observed with increasing weld width. Similarly, fatigue damage increase is observed with an increase of length of the cantilever beam.

The impact of safety factors was examined more closely and independently of the geometry. The values of the Wöhler curve are decreased due to the safety factor (Fig. 7). The higher the safety factor, the lower the values of the relevant stress range. However, the calculation has taken into account the block of loading history (Fig. 1).

Fig. 9(d) can be constructed independently of the geometry of cantilever beam, only the observed geometrical detail and load with the categories of construction details $\Delta\sigma_C$=36 MPa and $\Delta\tau_C$=80 MPa are considered as a condition. This graph can be made for any block of loading history and constructional detail category and afterwards used with structural analysis to find the suitable stress inducing lower fatigue damage. It is observed that the greater impact on fatigue damage comes from the safety factor and the angle of cross-section. Figs. 10(a) and 10(b) show the variation of the damage accumulation depending on the chosen parameter and variable ranges at location P6. Similar diagrams are observed for other locations.

The fatigue damage range is defined as the absolute difference between the minimum and maximum fatigue damage of one parameter. By dividing the fatigue damage range by the initial fatigue damage (see Eq. (16)), an influence factor (Fatigue damage influence factor-FDIF) is then defined, that can be assigned to each parameter.

$$FDIF = \frac{|D_H - D_L|}{D_0} \tag{16}$$

A higher factor means that a parameter in its defined range (Table 5) has a higher influence on the calculated fatigue damage for the block of the load history (Figs. 10 and 11(a)).

With taking into consideration the calculated critical stress, fatigue damage was calculated with each one of the safety factors ($\gamma_{Mf}$) and divided by fatigue damage calculated with $\gamma_{Mf}$=1.25 and initial values of the parameter (Table 3). For this parameter, the influence factor was defined differently by Eq. (17)

$$FDIF = \frac{D_{\gamma_{Mf}}}{D_0} \quad (17)$$

Note that this factor applies only for this stress and measured load specific. If the stress were higher, the difference would increase (see Fig. 9(d)).

At a normal stress of 80 MPa the difference in damage between the lowest and highest safety factors is more than double (Fig. 9(d)). If the calculated damage is compared when the variable is the safety factor only, fatigue damage rises with the increase of safety factor. A higher overall stress increases the impact of the higher safety factor (Figs. 10(a)-(b) and Fig. 11(b).

This difference can mean that choosing an inappropriate safety factor can lead to large deviations in endurance prediction.

## 4. Conclusions

In this paper, fatigue damage evaluations have been performed to investigate the influence of the geometry of a welded cantilever beam. In addition the influence of the safety factor, as defined by Eurocode 3, was examined.

The following conclusions can be made:

- It is observed that the calculated fatigue damage deviates considerably with the choice of the endurance safety factor. With a safety factor of 1.35, there is more than 4 times the fatigue damage computed than with a safety factor of 1.0.
- When considering the angle of the critical cross-section, the length of the cantilever beam and the weld thickness, the study has shown that the angle of cross-section has the biggest influence on fatigue damage calculation.
- When considering the weld width of the critical cross-section, changes in fatigue damage are nonlinear and the fatigue damage approaches a lower limit as greater weld widths are considered. Similarly, an increase of cantilever beam length causes the fatigue damage to increase with a non-linear trend.
- As the geometry influences fatigue damage predictions in a similar way as the endurance safety factor, a geometry factor could be established between different geometries of the cantilever beam, assessment method and consequence of failure to substitute repetitions of structural analyses for potential changes of the geometry.

## Acknowledgments

This paper is a part of research work within the program Nr. P2-0182 entitled Development evaluation financed by the Slovenian Research Agency. The authors are very grateful for the financial support.

## References

Akrache, R. and Lu, J. (2011), "Integrated design for fatigue life estimation of structures", *J. Mech. Eng.*, **57**(8), 547-554.

Altunisik, A.C., Ates, S. and Husem, M. (2016), "Lateral buckling of steel cantilever roof of a tribune due to snow loads", *Eng. Fail. Analy.*, **77**, 67-78.

Altunisik, A.C., Bayraktar, A., Sevim, B., Adanur, S. and Domanic, A. (2010), "Construction stage analysis of Komurhan Highway Bridge using time dependent material properties", *Struct. Eng. Mech.*, **36**(2), 207-233.

Anwar, W., Khan, M.Z., Israr, A., Mehmood, S. and Anjum, N.A. (2017), "Effects of structural dynamical characteristics and damage tolerance of aerospace grade composite materials", *Aerosp. Sci. Technol.*, **64**(5), 39-51.

Eurocode (2005), *Eurocode 3: Design of Steel Structures, Part 1-9: Fatigue*, European Committee for Standardization, Brussels, Belgium.

Fokter, S.K, Moličnik, A., Kavalar, R., Pelicon, P., Rudolf, R. and Gubeljak, N. (2017), "Why do some titanium-alloy total hip arthoplasty modular necks fail?", *J. Mech. Behav. Biomed. Mater.*, **69**, 107-114.

Gonzalez-Cruz, C.A. (2016), "Nonlinear response of cantilever beams due to large geometric deformations: Experimental deformations", *J. Mech. Eng.*, **62**(3), 187-196.

Granata, M.F., Margiotta, P., Recupero, A. and Arici, M. (2013), "Concrete arch bridges built by lattice cantilevers", *Struct. Eng. Mech.*, **45**(5), 703-722.

Griza, S., Dos Santos, S.V., Ueki, M.M., Bertoni, F. and Strohaecker, T.R. (2013), "Case study and analysis of fatigue failure in a THA stem", *Eng. Fail. Analy.*, **28**, 166-175.

Ingole, S.B. and Chatterjee, A. (2015), "Structural joint modeling and identification: Numerical and experimental investigation", *Struct. Eng. Mech.*, **53**(2), 373-392.

Iwicki, P., Rejowski, K. and Tejchman, J. (2015): "Stability of cylindrical steel silos composed of corrugated sheets and columns based on FE analyses versus Eurocode 3 approach", *Eng. Fail. Analy.*, **57**, 444-469.

Liu, J., Zhu, W.D., Charalambides, P.G., Shao, Y.M., Xu, Y.F. and Fang, X.M. (2016), "A dynamic model of a cantilever beam with a closed, embedded horizontal crack including local flexibilities at crack tips", *J. Sound Vibr.*, **382**, 274-290.

Marsh, G., Wignal, C., Thies, P.R., Barltrop, N., Incecik, A., Venugopal, V. and Johanning, L. (2016), "Review and application of Rainflow residue processing techniques for accurate fatigue damage estimation", *Int. J. Fatig.*, **82**, 757-765.

Nussbaumer, A., Borges, L. and Davaine, L. (2011), *Fatigue Design of Steel and Composite Structures: Eurocode 3: Design of Steel Structures, Part 1-9 Fatigue, Eurocode 4: Design of Composite Steel and Concrete Structures*, Wiley, Berlin, Germany.

Paulus, M. and Dasgupta, A. (2012), "Semi-empirical life model of a cantilever beam subject to random vibration", *Int. J. Fatig.*, **45**, 82-90.

Radaj, D. (2003), *Welding Residual Stresses and Distortion, Calculation and Measurement*, DVS Verlag, Düsseldorf, Germany.

Saranik, M., Jezequel, L. and Lenoir, D. (2013), "Experimental

and numerical study for fatigue life prediction of bolted connection", *Proc. Eng.*, **66**, 354-368.
Savković, M., Gašić, M., Petrović, D., Zdravković, N. and Pljakić R. (2011), "Analysis of the drive shaft fracture of the bucket wheel excavator", *Eng. Fail. Analy.*, **20**, 105-117.
Schijve, J. (2009), *Fatigue of Structures and Materials*, Springer, Netherlands.
Sedlacek, G. and Kraus, O. (2007), "Use of safety factors for the design of steel structures according to the Eurocodes", *Eng. Fail. Analy.*, **14**(3), 413-441.
Šeruga, D., Fajdiga, M. and Nagode, M. (2011), "Creep damage calculation for thermo mechanical fatigue", *J. Mech. Eng.*, **57**(5), 371-378.
Šeruga, D., Hansenne, E., Haesen, V. and Nagode, M. (2014), "Durability prediction of EN 1.4512 exhaust mufflers under thermo mechanical loading", *Int. J. Mech. Sci.*, **84**, 199-207.
Shi, Z. and Nakano, M. (2001), "Application of a 3-D crack analysis model to RC cantilever decks of excessive cracking", *Struct. Eng. Mech.*, **12**(4), 377-396.
Sondej, M., Iwicki, P., Michał, W. and Tejchman, J. (2016), "Stability analyses of cylindrical steel silos with corrugated sheets and columns", *Steel Compos. Struct.*, **20**(1), 147-166.
Totten, G. (2008), "Fatigue crack propagation", *Adv. Mater. Proc.*, **166**(5), 39-41.
Wang, B., Lu, G. and Yu, T.X. (1995), "A numerical analysis of the large deflection of an elastoplastic cantilever", *Struct. Eng. Mech.*, **3**(2), 163-172.
Zaletelj, H., Fajdiga, G. and Nagode, M. (2011), "Numerical methods for TMF cycle modeling", *J. Mech. Eng.*, **57**(6), 485-494.
Zeng, J., Ma, H., Zhang, W. and Wen, B. (2017), "Dynamic characteristic analysis of cracked cantilever beams under different crack types", *Eng. Fail. Analy.*, **74**, 80-94.

*PL*